

# Characterization of a Hexagonal Phosphorus Adlayer on Platinum (111)

Olli Heikkinen,<sup>†</sup> Hugo Pinto,<sup>‡</sup> Godhuli Sinha,<sup>†</sup> Sampsa K. Hämäläinen,<sup>†</sup> Jani Sainio,<sup>†</sup> Sven Öberg,<sup>§</sup> Patrick R. Briddon,<sup>||</sup> Adam S. Foster,<sup>‡</sup> and Jouko Lahtinen<sup>\*,†</sup>

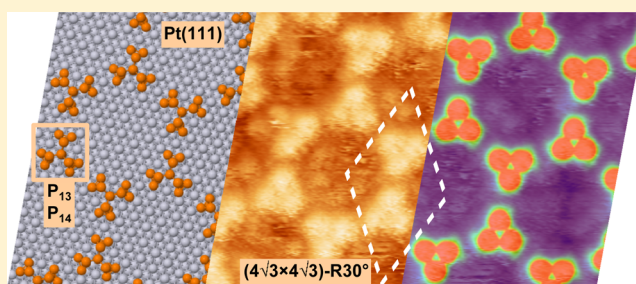
<sup>†</sup>Department of Applied Physics, Aalto University School of Science, P.O. Box 14100, FI-00076 Aalto, Finland

<sup>‡</sup>COMP Centre of Excellence, Department of Applied Physics, Aalto University School of Science, P.O. Box 11100, FI-00076 Aalto, Finland

<sup>§</sup>Department of Engineering Sciences and Mathematics, Luleå University of Technology, Luleå S-97187, Sweden

<sup>||</sup>School of Electrical and Electronic Engineering, Newcastle University, Newcastle upon Tyne, NE1 7RU, United Kingdom

**ABSTRACT:** Platinum is a well-known catalytic metal whose efficiency can be degraded by the adsorption of impurities. Using different characterization techniques, such as scanning tunnelling microscopy, low-energy electron diffraction, and X-ray photoelectron spectroscopy, we present a study of phosphorus adsorption on a platinum (111) surface. Under saturation and after annealing at 750 °C, phosphorus was observed to form an ordered hexagonal adlayer with a  $(4\sqrt{3} \times 4\sqrt{3})\text{-R}30^\circ$  symmetry. On the basis of density functional theory calculations, we propose a model for the phosphorus adlayer, consisting of either  $\text{P}_{13}$  or  $\text{P}_{14}$  clusters. In addition, carbon monoxide adsorption as a function of the phosphorus coverage was also investigated. We found that the phosphorus adlayer prevents carbon monoxide adsorption on Pt(111) reducing its catalytic efficiency.



## INTRODUCTION

Due to its exceptional catalytic properties, platinum is a widely used metal in technologically important catalytic processes. For instance, its high efficiency in oxidizing carbon monoxide makes platinum a commonly used material in catalytic converters on combustion engines. However, the catalytic activity of platinum can be affected by sintering, phase transformation, and poisoning.<sup>1</sup> The latter is caused by the chemisorption of impurities which can block the active sites<sup>2</sup> or change the electronic structure of the surface atoms.<sup>3</sup> In car exhaust catalysts, fuels, additives, and lubricants are sources of impurities such as sulfur and phosphorus. Thus, understanding of the reactions between the impurities and the surface is crucial in order to reduce the aging of catalytic converters.

Of the two catalytic poisons mentioned above, sulfur has been studied more extensively in the past.<sup>1,4,5</sup> Both sulfide and sulfate species have been reported to cause blocking of active sites,<sup>4</sup> but in most studies, sulfur does not significantly alter the chemical state of the active metal (Pt).<sup>5</sup> Adsorption of sulfur and its effects on CO adsorption have also been studied in ideal model systems. On a Pt(111) single crystal surface, CO forms ordered overlayers. CO molecules prefer bonding to on-top sites, but when the coverage is above 0.17 ML, also bridge sites are occupied.<sup>6</sup> A  $(2 \times 2)$  overlayer of sulfur on a Pt(111) surface has been observed to reduce CO intake, whereas a  $(\sqrt{3} \times \sqrt{3})\text{-R}30^\circ$  adlayer blocks the CO adsorption altogether.<sup>7</sup>

Phosphorus poisoning, on the other hand, has not been studied as thoroughly. The majority of it is adsorbed as phosphates on the catalyst surface; e.g., on alumina supported palladium catalysts, phosphorus has been detected as a mixed overlayer of metal phosphates and  $\text{AlPO}_4$  in the uppermost layer of the washcoat.<sup>1,8</sup> On Pt/ $\text{Al}_2\text{O}_3$  and PtPd/ $\text{Al}_2\text{O}_3$  catalysts, phosphorus has been observed to decrease CO, NO, and  $\text{C}_3\text{H}_6$  oxidation activity.<sup>9</sup>

Previously, adsorption of hydrogen phosphates in acidic solutions on a Pt(111) surface has been studied with vibrational infrared spectroscopy, cyclic voltammetry, and thermodynamic calculations.<sup>10–12</sup> In these studies, which have aimed at development of fuel cells and biosensors, deprotonation from  $\text{H}_2\text{PO}_4^-$  to  $\text{HPO}_4^{2-}$  and further to  $\text{PO}_4^{3-}$  has been observed in the adsorbates.

There are hardly any earlier structural studies of phosphorus on metallic single crystals. On the other hand, on semiconductor surfaces, especially on Si(100), adsorption structures of phosphorus have been studied in more detail. In a combined STM and DFT study,  $\text{P}_2$  molecules from a solid indium phosphide source have been observed to adsorb on Si(100) on four different sites, whereas  $\text{P}_4$  has only one preferred site.<sup>13</sup> On germanium (111), phosphorus adsorbs as  $\text{P}_3$  trimers and locally

Received: December 19, 2014

Revised: May 8, 2015

Published: May 8, 2015

forms a ( $\sqrt{3} \times \sqrt{3}$ )-R30° adlayer, lacking however a long-range order.<sup>14</sup> The sparsity of previous studies makes phosphorus an interesting topic from a scientific point of view. Furthermore, the recent discovery of “phosphorene”, a semiconducting monolayer of black phosphorus,<sup>15</sup> encourages investigating phosphorus structures also in the perspective of nanotechnology.

In the present work, adsorption of molecular phosphorus evaporated from a solid red phosphorus source on Pt(111) is studied in ultrahigh vacuum (UHV). The emphasis is on studying the adsorption structure with scanning tunnelling microscopy (STM) together with density functional theory (DFT) calculations. Carbon monoxide adsorption on a phosphorus precovered surface has also been investigated to gain insight into the poisoning effect in idealized conditions.

## METHODS

**Experimental Details.** All the experiments were carried out in two UHV systems. Structural characterization with STM and low-energy electron diffraction (LEED) was carried out in a UHV system consisting of a variable temperature STM (RHK UHV750), LEED optics (Omicron SpectraLEED), and a DPCMA electron spectrometer (Physical Electronics 15-255G) for Auger electron spectroscopy (AES). The base pressure in the system is  $5 \times 10^{-11}$  mbar. For sample preparation, the system features a sputtering ion gun (Varian), liquid nitrogen cooling, and electron beam heating.

Phosphorus coverage characterization with X-ray photoelectron spectroscopy (XPS) and carbon monoxide adsorption experiments were carried out in another UHV system with a base pressure of  $1 \times 10^{-10}$  mbar. The chamber features a hemispherical analyzer and a dual anode X-ray source (Physical Electronics 3057) for XPS and LEED optics (PRI, RVL 8-120) as well as a quadrupole mass spectrometer (Stanford Research Systems RGA100). For sample preparation, the chamber is equipped with a differentially pumped ion gun (Physical Electronics), liquid nitrogen cooling, and resistive heating.

The platinum crystals used in this study have been acquired from MaTeck GmbH. In both systems, sample cleaning was carried out by repeated cycles of sputtering ( $\text{Ar}^+$  ions, 15 min, 2 kV) and annealing (20 min, 900 °C). AES or XPS together with LEED were used to monitor the quality of the surface.

Red phosphorus powder (Aldrich, purity  $\geq 99.99\%$ ) was inserted in a steel container which was connected to the UHV chamber through a leak valve. This setup was identical in both systems. During the exposure, the pressure in the container was first pumped down to  $1 \times 10^{-2}$  mbar and then the temperature of the container was increased with a heating gun up to ca. 500 °C so that the pressure increased above 1 mbar. At temperatures below 800 °C, phosphorus vapor mainly consists of  $\text{P}_4$  molecules. Above 800 °C,  $\text{P}_4$  starts to dissociate to  $\text{P}_2$ .<sup>16</sup> The platinum crystal was facing a nozzle connected to the leak valve guiding phosphorus vapor toward the crystal enabling us to get much larger local exposure than what could be achieved by backfilling the chamber. The exposure with the nozzle was not calibrated, but AES and XPS were used directly for coverage determination.

Carbon monoxide (AGA, purity 99.997%) was introduced through a leak valve backfilling the chamber. The adsorption was carried out at room temperature.

**Computational Details.** The adsorption of phosphorus on the Pt(111) surface was studied using the density functional theory (DFT) within the generalized gradient approximation

(GGA)<sup>17</sup> with dispersion corrections (DFT-D2)<sup>18</sup> as implemented in the AIMPRO code.<sup>19</sup> The core electrons of the atoms were replaced by the Hartwigsen Goedecker Hutter (HGH) pseudopotentials,<sup>20</sup> while the orbitals of the valence electrons consist of independent s-, p-, and d-like Gaussian functions centered on atoms.<sup>21</sup> With the basis chosen to describe the Pt atoms, the calculated lattice parameter and bulk modulus for bulk fcc Pt are 3.94 Å and 239 GPa, respectively. Compared with the experimental values (3.92 Å and 230 GPa<sup>22</sup>), the error in our calculations is smaller than 1%, suggesting that the basis set used is large enough to correctly reproduce the bulk properties of Pt. Charge density was Fourier-transformed using plane waves with an energy cutoff of 100 Ha. The Kohn–Sham levels were calculated using metallic filling with Fermi–Dirac statistics,  $k_B T = 0.04$  eV. For the sampling of the Brillouin zone, we used a grid of  $2 \times 2 \times 1$  k-points within the Monkhorst–Pack scheme<sup>23</sup> ensuring the convergence of the total energy within about 0.02 eV.

First, the structural properties and the energetics of isolated phosphorus clusters  $\text{P}_n$  ( $n = 2-14$ ) were investigated. The structures of interest were then placed on top of a Pt(111) surface and the atomic positions optimized. The surface was modeled using a four-layer Pt slab, enclosing 192 atoms, the optimal thickness needed to reproduce the properties of the Pt(111) surface.<sup>24</sup> In the direction perpendicular to the surface, a vacuum layer of 13 Å was placed to avoid the interaction between surfaces in neighboring cells. During the structure relaxation, the two bottom layers were fixed while all the other atoms were allowed to move until the forces acting on each atom were less than  $3 \times 10^{-3}$  eV/Å.

The stability of the different clusters was compared in terms of its formation energy  $E_f$  defined by  $E_f = E_n - n\mu_P$ . Here  $E_n$  is the total energy of a cluster containing  $n$  phosphorus atoms and  $\mu_P$  the chemical potential for the phosphorus atom.  $\mu_P$  was estimated from the total energy  $E_T$  of the tetrahedral  $\text{P}_4$  according to  $\mu_P = E_T/4$ .

The occurrence and direction of charge transfer at the metal/phosphorus interface was investigated by comparing the highest occupied molecular orbital (HOMO) and lowest unoccupied molecular orbital (LUMO) levels of the phosphorus clusters to the Fermi level of the clean Pt(111) surface. Additionally, Bader charge analysis was employed to estimate the amount of charge transfer between the clusters and the surface.<sup>25-27</sup>

Finally, simulated STM images were obtained by plotting an iso-surface electron density within the vicinity of the Fermi energy at a specific height above the surface.

## RESULTS

**Phosphorus Adlayer Characterization with Experimental Methods.** Phosphorus adsorption was performed both at room temperature and at 450 °C. The results indicate that the sticking was larger by a factor of 7 at elevated temperature. This further indicates that overcoming an activation energy of approximately 10 meV is needed for the adsorption to take place. Onward, all the adsorption experiments were carried out while having the surface at 450 °C. A saturation coverage was achieved featuring a P 2p to Pt 4f<sub>7/2</sub> line intensity ratio of  $0.020 \pm 0.002$  in XPS.

After saturation, some diffraction spots of the adsorbate layer were observed with LEED, but the pattern was unclear and blurred. Substrate spots could not be seen at all. Annealing at 750 °C for 2 min led to a clear, ordered structure. After annealing, the P 2p to Pt 4f<sub>7/2</sub> line intensity ratio was  $0.012 \pm$

0.002, indicating removal of roughly 40% of the initial P on the surface. Temperature-programmed desorption (TPD) showed a phosphorus peak above 700 °C. On the other hand, phosphorus is a major impurity in high-purity platinum crystals,<sup>28</sup> and therefore, the reduction in phosphorus photoelectron intensity could also be due to phosphorus diffusing into the platinum bulk. To test the potential diffusion into the bulk, we measured the peak-to-background ratio of the P 2p peak to detect any increase in the inelastic scattering due to deep residing P atoms. However, such an effect was not observed, indicating that most of the phosphorus leaves the surface by desorption.

After annealing, LEED shows a  $(4\sqrt{3} \times 4\sqrt{3})\text{-R}30^\circ$  superstructure (Figure 1). In STM, an ordered, hexagonal

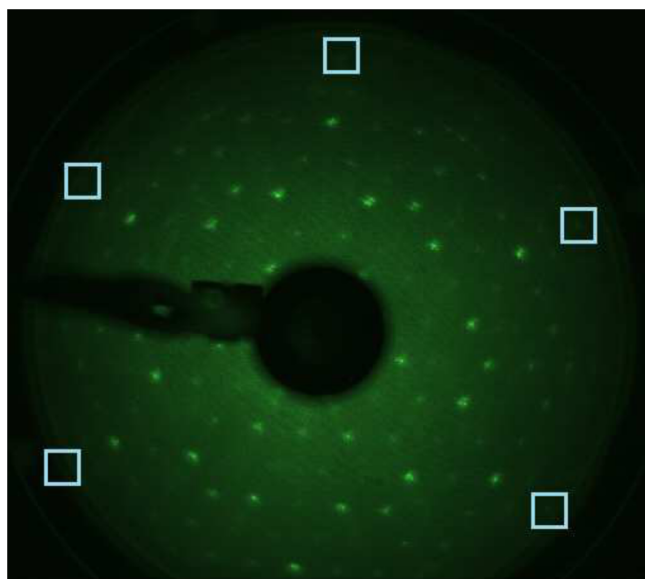


**Figure 1.** LEED pattern of a Pt(111) surface with a saturated phosphorus adlayer exhibiting  $(4\sqrt{3} \times 4\sqrt{3})\text{-R}30^\circ$  symmetry. The incident electron energy is 56 eV. Locations for the  $1 \times 1$  spots have been marked.

structure consisting of triangular clusters surrounded by less decorated areas was observed (Figure 2). The side length of the unit cell in the STM images is  $20 \pm 1 \text{ \AA}$  in both directions. The reported atomic separation on the Pt(111) surface is 2.77 Å.<sup>29</sup> Thus, for a  $(4\sqrt{3} \times 4\sqrt{3})\text{-R}30^\circ$  structure, the length of the lattice vector is 19.2 Å, which is in line with the STM results. All STM images within a bias range from  $-0.28$  to 0.65 V showed similar features.

A free  $\text{P}_4$  molecule has a bond length of 2.21 Å.<sup>30</sup> The triangular clusters in the STM images are significantly larger than that, indicating more complicated structures. We estimated the XPS intensity ratio between P 2p and Pt 4f<sub>7/2</sub> to be 0.002 if each triangular cluster observed in STM were a  $\text{P}_4$  molecule and if there were no other phosphorus particles on the surface. However, the observed ratio was remarkably higher, further implying larger phosphorus clusters. Since the annealing temperature is close to 800 °C, both  $\text{P}_4$  and  $\text{P}_2$  can be assumed to be present. Therefore, the structures are possibly combinations of them both. Inside the darker areas, additional features of varying brightness are visible.

**Phosphorus Adlayer Characterization by DFT.** In order to model the phosphorus molecular structures observed by STM on top of the Pt(111) surface, we first investigated the

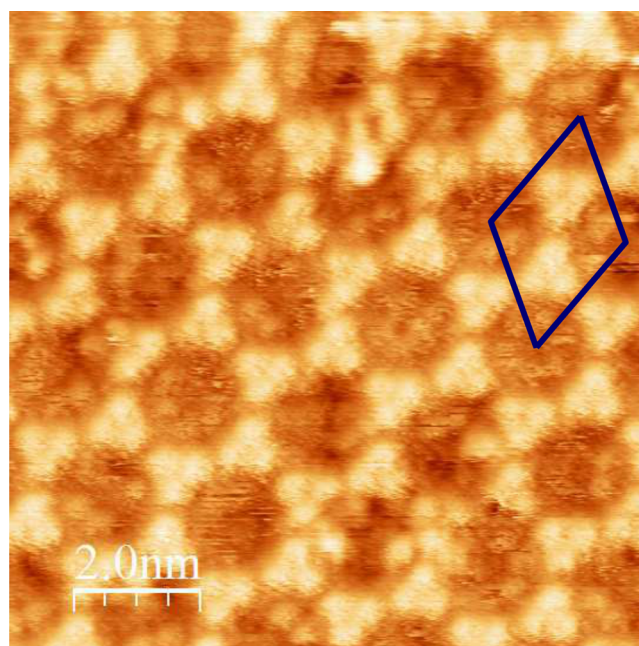


**Figure 2.** STM image of a Pt(111) surface with a saturated phosphorus adlayer with sample bias and tunnelling current of 62 mV/0.42 nA. Phosphorus forms a hexagonal superstructure consisting of triangular clusters surrounded by circular pores. The unit cell of the superstructure is shown.

geometry and formation of isolated phosphorus clusters. Phosphorus is an element in group 15 of the periodic table with three unpaired electrons in the valence 3p orbital available for bonding. Therefore, the preference for 3-fold coordination we found in studied phosphorus aggregates was perhaps not surprising. Additionally, our calculations show that 4-fold coordination is unstable while 2-fold coordination is energetically less favorable. In agreement with previous studies, we found that neutral phosphorus clusters with an even number of atoms are energetically more favorable than the odd numbered ones.<sup>31,32</sup>

Henceforth, we focus our attention on the plausible clusters that may be in the origin of the hexagonal structure. The tetrahedral  $\text{P}_4$  is the most stable phosphorus aggregate. Consisting of four phosphorus atoms each bound to three other atoms, as shown in Figure 3a, the cluster is stable until

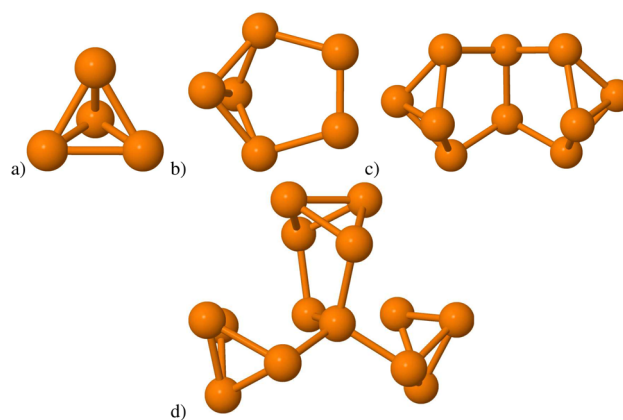


**Figure 3.** Calculated structures for the (a) tetrahedral  $\text{P}_4$ , (b)  $\text{P}_6$ , (c)  $\text{P}_{10}$ , and (d)  $\text{P}_{14}$  phosphorus clusters.

800 °C.<sup>16</sup> Above this temperature, it dissociates into P<sub>2</sub> units, the formation energy of which was estimated to be 1.5 eV higher with respect to the tetrahedral P<sub>4</sub>.

The P<sub>6</sub> cluster, shown in Figure 3b, can be derived from a P<sub>4</sub> unit and a P<sub>2</sub> dimer. The predicted formation energy for the P<sub>6</sub> lies 1.0 eV above the tetrahedral P<sub>4</sub>. Due to its size and symmetry, the P<sub>6</sub> cluster is insufficient to explain the experimental findings. Most similar to P<sub>4</sub> is the P<sub>10</sub> cluster which can be seen as two P<sub>4</sub> units connected by a P<sub>2</sub> dimer, as shown in Figure 3c. Each atom is bound to three other phosphorus atoms which makes the P<sub>10</sub> energetically as stable as the tetrahedral P<sub>4</sub>. Although the size of the P<sub>10</sub> is comparable to the structures observed on top of the Pt(111) surface, its shape cannot describe the pattern observed experimentally.

However, the desired symmetry can be achieved by binding an additional P<sub>4</sub>. Figure 3d shows the molecular structure of the P<sub>14</sub> made by a P<sub>2</sub> dimer surrounded by three P<sub>4</sub> units. The 4-fold coordination imposed to the P<sub>2</sub> dimer causes a rotation of the P<sub>4</sub> in the *x*–*y* plane which consequently lowers its symmetry. Although the formation of the P<sub>14</sub> is unlikely to occur in the gas phase, in the presence of the Pt(111) surface, the cluster remains stable. The size and the symmetry of the P<sub>14</sub> are in agreement with the structures visible in the STM scans. The P<sub>14</sub> cluster has four P atoms bonding with Pt atoms 2.65 Å above the surface with a binding energy of 6.16 eV (Table 1). The P<sub>2</sub> dimer in the middle of the cluster stands perpendicular to the surface at the on-top site. The bonding P atom in each P<sub>4</sub> unit resides nearly at the on-top site.

**Table 1. Binding Energies (eV) for the Phosphorus Clusters on the Pt(111) Surface**

cluster	binding energy	
	eV	eV/P atom
P <sub>4</sub>	1.09	0.27
P <sub>6</sub>	3.97	0.66
P <sub>10</sub>	4.27	0.43
P <sub>13</sub>	7.15	0.55
P <sub>14</sub>	6.16	0.44

In order to model the unit cell of the phosphorus pattern observed in the experiments, two P<sub>14</sub> clusters were placed in opposite orientations on top of a  $(4\sqrt{3} \times 4\sqrt{3})\text{-R}30^\circ$  Pt(111) slab. The optimized structure is shown in Figure 4. Repeating the unit cell in the *x* and *y* directions produces a hexagonal pattern consistent with the experimental observations. The lattice vector length of the theoretical phosphorus pattern is 19.7 Å, which is in perfect agreement with the 20 Å measured experimentally.

A similar agreement with the experiments is obtained if the P<sub>2</sub> dimer in the cluster is replaced by a single P atom, thus creating a P<sub>13</sub> cluster. Although the P<sub>13</sub> cluster is not stable in a vacuum, when adsorbed on the Pt(111) surface the cluster adopts a perfectly symmetrical triangular geometry, as shown in Figure 5. The P<sub>13</sub> cluster has three P atoms bonding with Pt 2.11 Å above the surface with a binding energy of 7.15 eV (Table 1). The binding energy is 1 eV larger than that of P<sub>14</sub>, indicating a more stable structure. The bonding P atom in each P<sub>4</sub> unit resides asymmetrically at the bridge site.

Figure 6 shows the energy level diagram of the HOMO and LUMO levels of the P<sub>13</sub> and P<sub>14</sub> together with the density of states (DOS) of Pt(111). The molecular energy levels are plotted relative to the Fermi level of the metallic substrate. For

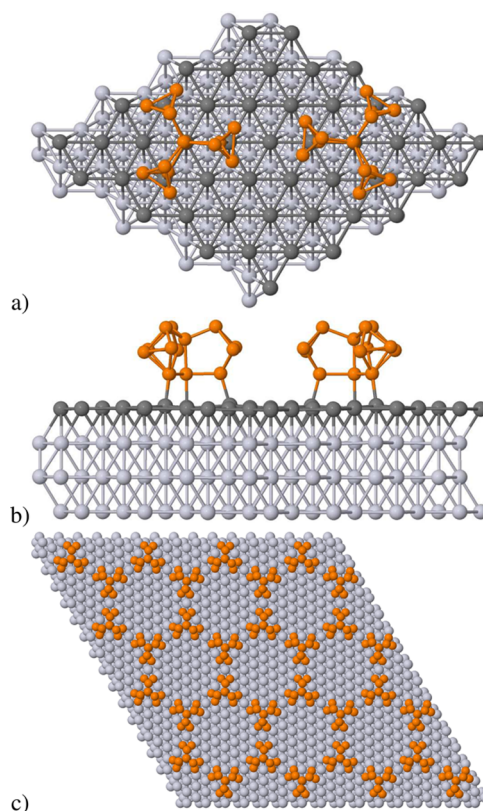


**Figure 4.** (a) Top and (b) side views of the unit cell of the hexagonal phosphorus pattern on top of the Pt(111) surface made by two P<sub>14</sub> units. (c) A hexagonal pattern is also seen by repeating the unit cell in the *x*- and *y*-directions. The lattice vector of the pattern is in perfect agreement with the experiments.

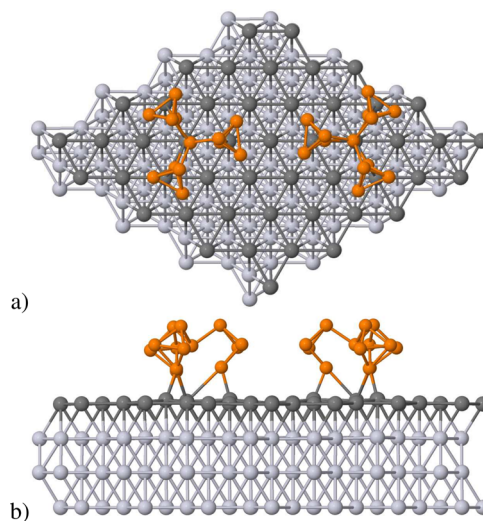


**Figure 5.** (a) Top and (b) side views of the unit cell of the hexagonal phosphorus pattern on top of the Pt(111) surface made by two P<sub>13</sub> units.

both clusters, P<sub>13</sub> and P<sub>14</sub>, the HOMO level lies above the Fermi level of the metallic substrate, suggesting a charge transfer between the phosphorus clusters and the Pt(111) surface. From Bader analysis, we estimate that a charge of approximately 0.80 and 0.86 electrons is transferred to the Pt from the P<sub>13</sub> and P<sub>14</sub> clusters, respectively.

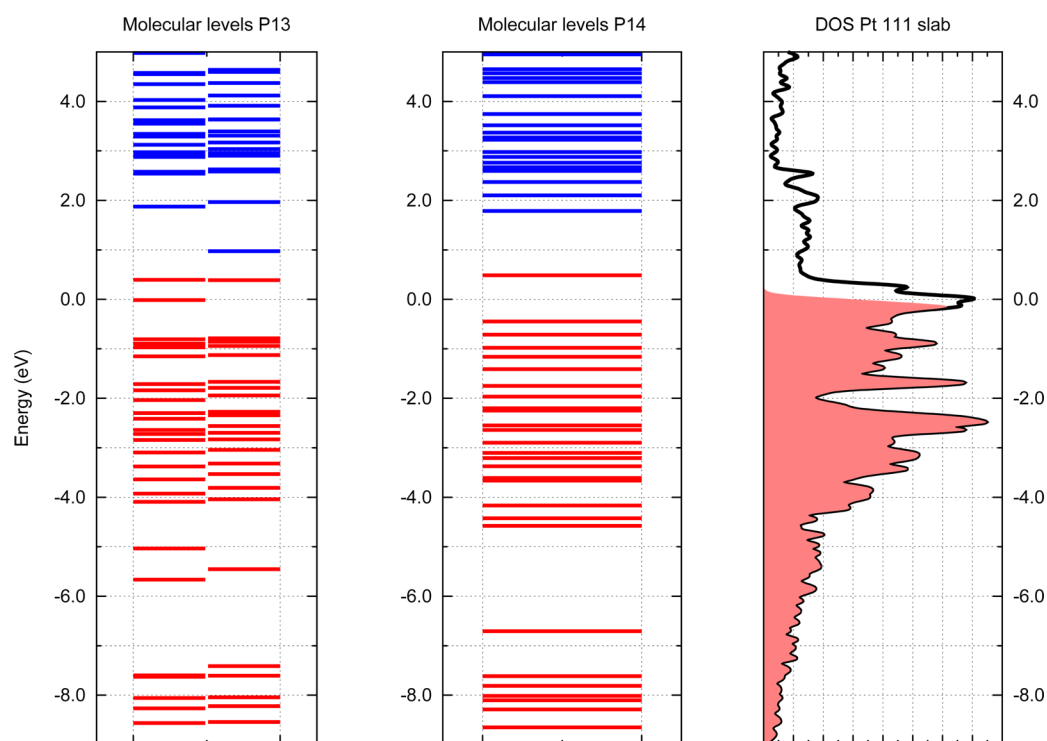


**Figure 6.** Plot of the HOMO and LUMO levels of the  $P_{13}$  and  $P_{14}$  together with the DOS of the Pt(111) slab. The zero energy is set to the Fermi level of the Pt(111) slab. Filled and empty molecular levels are represented in red and blue, respectively, while the red shaded area in the DOS represents the filled states of the Pt(111) slab. For the  $P_{13}$ , the left and right energy levels represent spin-up and spin-down states, respectively.

In order to get a direct comparison with the experimental measurements, STM plots for both  $P_{13}$  and  $P_{14}$  patterns were calculated. The STM images were calculated from a 2D projection of the charge density of the occupied levels 2 eV below the Fermi energy. For simplicity, the images were produced 5 Å above the surface in the absence of the metallic slab. However, the features of the images presented here do not change for the range of heights usually used in STM measurements or if the metallic slab is included in the calculations. Both simulated images show a hexagonal pattern overlapping the atomic phosphorus structure. Similarly to the experiments, the individual clusters are denoted by three-pointed structures with a bright spot at each corner, as seen in Figure 7. Furthermore, adjacent clusters are separated by a clear

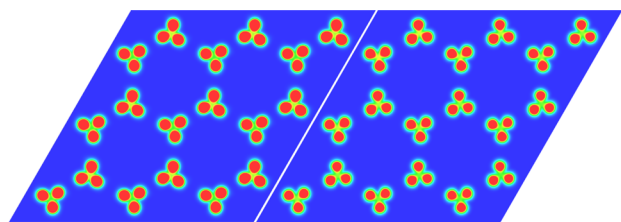


**Figure 7.** Simulated STM images for  $P_{13}$  (left) and  $P_{14}$  (right) overlayers.

narrow gap forming a mosaic-like pattern. The match between the simulated and experimental STM shown in Figure 8 provides strong evidence that the hexagonal phosphorus pattern can be modeled either by  $P_{13}$  or  $P_{14}$  clusters.

Furthermore, calculations suggest that the additional spots observed inside the pores can be explained by the presence of trapped  $P_4$  clusters. Indeed, the STM features produced by an

unbound  $P_4$  cluster, as seen in Figure 8, are similar to the adjacent structures observed experimentally.

**Carbon Monoxide Adsorption on a P/Pt Surface.** In order to study catalytic poisoning, carbon monoxide adsorption (with 1.5 L of CO exposure) was investigated with XPS and TPD as a function of phosphorus coverage after phosphorus deposition and annealing. In XPS, the carbon 1s line was measured before and after CO exposure and its growth was attributed to the CO intake. In TPD, molecular desorption of CO ( $m/z = 28$ ) at 100 °C was observed. In Figure 9, the growth in the C 1s XPS line as well as the desorption yield of CO are shown as a function of phosphorus coverage relative to the saturated coverage.

Both XPS and TPD indicate that carbon intake reduces linearly as the phosphorus coverage grows. At saturation coverage, CO adsorption vanishes altogether. The CO adsorption measurement at saturated P coverage was carried out using a CO exposure of 15 L to ensure that the decreased adsorption is due to blocking of the adsorption sites and not due to decreased sticking probability of CO. No CO adsorption was detected. The inset in Figure 9 shows some of the CO desorption spectra. A smoothening function has been used to reduce noise in the spectra.

## DISCUSSION

Although the assumption that the phosphorus clusters are directly on top of Pt(111) provides a suitable model for the hexagonal pattern, the possibility of additional phosphorus on the surface cannot be excluded. We estimate that the intensity ratio between P 2p and Pt  $4f_{7/2}$  lines would be ca.  $0.008 \pm 0.002$  and  $0.009 \pm 0.002$  for the mere hexagonal pattern of  $P_{13}$  and  $P_{14}$  clusters, respectively. The estimated ratio for an overlayer with one P atom per one Pt surface atom is  $0.015 \pm$

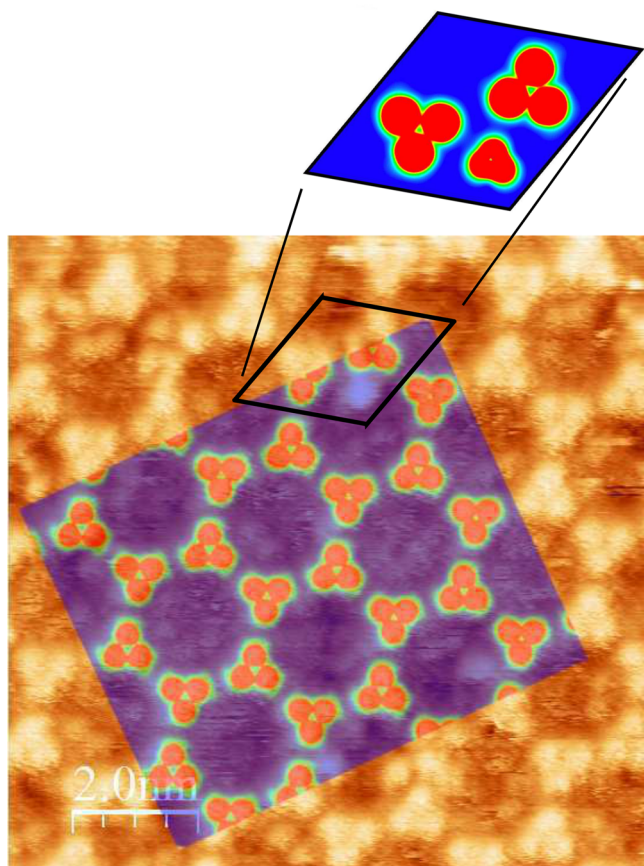


**Figure 8.** Comparison between the experimental and simulated STM images. The clusters in the simulated image are  $P_{13}$ . The topmost part shows a calculated STM image for an unbound  $P_4$  cluster adjacent to the phosphorus superstructure.

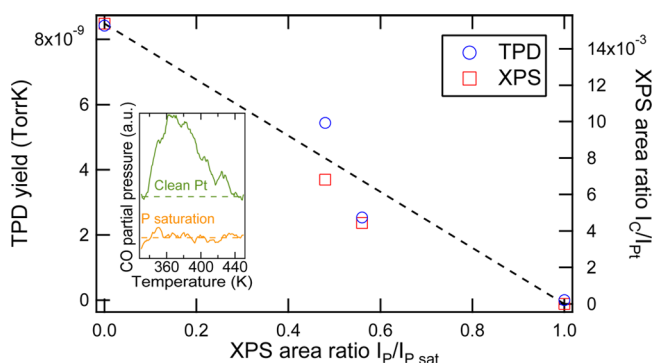


**Figure 9.** Carbon 1s XPS intensities (red) and carbon monoxide TPD yields (blue) as a function of phosphorus coverage. TPD spectra of carbon monoxide are shown in the inset.

0.003. The estimates were calculated using effective attenuation lengths, which leads to error bars of 20% or more.<sup>33</sup> The experimentally acquired XPS ratio  $0.012 \pm 0.002$  thus suggests that in addition to the hexagonal overlayer there is likely to be additional phosphorus on the surface. The zero CO intake at phosphorus saturation also supports this possibility. The excess is not necessarily large, and the extra clusters frequently observed in the STM scans, predicted to be  $P_4$  molecules trapped in a pore (Figure 8), may explain it altogether. On the basis of the XPS ratios, we cannot, however, rule out the possibility of some intermixing of phosphorus with the topmost

platinum layers. In order to get a detailed picture of the phosphorus Pt(111) interface, further studies, both experimental and theoretical, are required.

In summary, we have studied phosphorus adsorption on a platinum (111) single crystal surface both experimentally and computationally. On the basis of LEED, the structure was observed to have a symmetry of  $(4\sqrt{3} \times 4\sqrt{3})-R30^\circ$ . STM images show that the adlayer consists of three-pointed atomic clusters in a hexagonal pattern. By DFT calculations, a model with  $P_{13}$  or  $P_{14}$  clusters has been proposed. When the atomic positions are optimized, they form a pattern similar to the one observed in STM. The clusters do not exclude each other, and both may be present on the surface.

Carbon monoxide adsorption on a phosphorus covered Pt(111) surface was studied experimentally. Both XPS and TPD studies show that the saturated phosphorus overlayer totally prevents CO intake. Below the saturation limit, the intake drops linearly as a function of phosphorus coverage. Although the study was performed in an idealized setup, it gives some insight into more complex systems as well: also on supported Pt surfaces, phosphorus may form large clusters, thus blocking adsorption sites.

## AUTHOR INFORMATION

### Corresponding Author

\*E-mail: jouko.lahtinen@aalto.fi.

### Notes

The authors declare no competing financial interest.

## ACKNOWLEDGMENTS

This research has been supported by the Academy of Finland through the ACaBio project (No. 139187), Centres of Excellence Program (Project No. 251748), and EU project PAMS (Contract No. 610446). We acknowledge CSC – IT Center for Science Ltd. for the allocation of computational resources.

## REFERENCES

- (1) Neyestanaki, A. K.; Klingstedt, F.; Salmi, T.; Murzin, D. Y. Deactivation of Postcombustion Catalysts, a Review. *Fuel* **2004**, *83*, 395–408.
- (2) Bartholomew, C. H. Mechanisms of Catalyst Deactivation. *Appl. Catal., A* **2001**, *212*, 17–60.
- (3) Forzatti, P.; Lietti, L. Catalyst Deactivation. *Catal. Today* **1999**, *52*, 165–181.
- (4) Sedlmair, C.; Seshan, K.; Jentys, A.; Lercher, J. A. Studies on the Deactivation of  $NO_x$  Storage-Reduction Catalysts by Sulfur Dioxide. *Catal. Today* **2002**, *75*, 413–419.
- (5) Kärkkäinen, M.; Honkanen, M.; Viitanen, V.; Kolli, T.; Valtanen, A.; Huuhtanen, M.; Kallinen, K.; Vippola, M.; Lepistö, T.; Lahtinen, J.; et al. Deactivation of Diesel Oxidation Catalysts by Sulphur in Laboratory and Engine-Bench Scale Aging. *Top. Catal.* **2013**, *56*, 672–678.
- (6) Steininger, H.; Lehwald, S.; Ibach, H. On the Adsorption of CO on Pt(111). *Surf. Sci.* **1982**, *123*, 264–282.
- (7) Garfunkel, E. L.; Farias, M. H.; Somorjai, G. A. The Modification of Benzene and Carbon Monoxide Adsorption on Platinum(111) by the Coadsorption of Potassium or Sulfur. *J. Am. Chem. Soc.* **1985**, *107*, 349–353.
- (8) Rokosz, M. J.; Chen, A. E.; Lowe-Ma, C. K.; Kucherov, A. V.; Benson, D.; Peck, M. C. P.; McCabe, R. W. Characterization of Phosphorus-Poisoned Automotive Exhaust Catalysts. *Appl. Catal., B* **2001**, *33*, 205–215.
- (9) Kärkkäinen, M.; Kolli, T.; Honkanen, M.; Heikkinen, O.; Huuhtanen, M.; Kallinen, K.; Lepistö, T.; Lahtinen, J.; Vippola, M.;

Keiski, R. L. The Effect of Phosphorus Exposure on Diesel Oxidation Catalysts - Part I: Activity Measurements, Elementary and Surface Analyses. *Top. Catal.* **2015**, in press.

(10) Mostany, J.; Martínez, P.; Climent, V.; Herrero, E.; Feliu, J. M. Thermodynamic Studies of Phosphate Adsorption on Pt(1 1 1) Electrode Surfaces in Perchloric Acid Solutions. *Electrochim. Acta* **2009**, *54*, 5836–5843.

(11) Gisbert, R.; García, G.; Koper, M. T. M. Adsorption of Phosphate Species on Poly-Oriented Pt and Pt(1 1 1) Electrodes over a Wide Range of pH. *Electrochim. Acta* **2010**, *55*, 7961–7968.

(12) Weber, M.; Nart, F. C.; de Moraes, I. R. Adsorption of Phosphate Species on Pt(111) and Pt(100) as Studied by in Situ FTIR Spectroscopy. *J. Phys. Chem.* **1996**, *100*, 19933–19938.

(13) Sagisaka, K.; Marz, M.; Fujita, D.; Bowler, D. Adsorption of Phosphorus Molecules Evaporated from an InP Solid Source on the Si(100) Surface. *Phys. Rev. B: Condens. Matter Mater. Phys.* **2013**, *87*, 155316.

(14) Vitali, L.; Ramsey, M. G.; Netzer, F. P. Trimer Adatom Structure of Phosphorus on Ge(111). *Phys. Rev. B: Condens. Matter Mater. Phys.* **2001**, *63*, 165320.

(15) Li, L.; Yu, Y.; Ye, G. J.; Ge, Q.; Ou, X.; Wu, H.; Feng, D.; Chen, X. H.; Zhang, Y. Black Phosphorus Field-Effect Transistors. *Nat. Nanotechnol.* **2014**, *9*, 372–377.

(16) MacKay, K. M.; MacKay, R. A.; Henderson, W. *Introduction to Modern Inorganic Chemistry*, 6th ed.; CRC Press: Cheltenham, U.K., 2002.

(17) Perdew, J. P.; Burke, K.; Ernzerhof, M. Generalized Gradient Approximation Made Simple. *Phys. Rev. Lett.* **1996**, *77*, 3865.

(18) Grimme, S. Semiempirical GGA-Type Density Functional Constructed With a Long-Range Dispersion Correction. *J. Comput. Chem.* **2006**, *27*, 1787–1799.

(19) Jones, R.; Briddon, P. R. The Ab Initio Cluster Method and the Dynamics of Defects in Semiconductors. *Semicond. Semimetals* **1998**, *51*, 287–349.

(20) Hartwigsen, C.; Goedecker, S.; Hutter, J. Relativistic Separable Dual-Space Gaussian Pseudopotentials from H to Rn. *Phys. Rev. B: Condens. Matter Mater. Phys.* **1998**, *58*, 3641.

(21) Goss, J. P.; Shaw, M. J.; Briddon, P. R. Marker-Method Calculations for Electrical Levels Using Gaussian-Orbital Basis Sets. *Top. Appl. Phys.* **2007**, *104*, 69–94.

(22) Villars, P.; Calvert, L. *Pearson's Handbook of Crystallographic Data for Intermetallic Phases*, 2nd ed.; ASM International: Materials Park, OH, 1991.

(23) Monkhorst, H. J.; Pack, J. D. Special Points for Brillouin-Zone Integrations. *Phys. Rev. B: Condens. Matter Mater. Phys.* **1976**, *13*, 5188.

(24) Kokalj, A.; Causà, M. Periodic Density Functional Theory Study of Pt(111): Surface Features of Slabs of Different Thicknesses. *J. Phys.: Condens. Matter* **1999**, *11*, 7463–7480.

(25) Tang, W.; Sanville, E.; Henkelman, G. A Grid-Based Bader Analysis Algorithm without Lattice Bias. *J. Phys.: Condens. Matter* **2009**, *21*, 084204.

(26) Sanville, E.; Kenny, S. D.; Smith, R.; Henkelman, G. Improved Grid-Based Algorithm for Bader Charge Allocation. *J. Comput. Chem.* **2007**, *28*, 899–908.

(27) Henkelman, G.; Arnaldsson, A.; Jónsson, H. A Fast and Robust Algorithm for Bader Decomposition of Charge Density. *Comput. Mater. Sci.* **2006**, *36*, 354–360.

(28) Musket, R. G.; McLean, W.; Colmenares, C. A.; Makowiecki, D. M.; Siekhaus, W. J. Preparation of Atomically Clean Surfaces of Selected Elements: A Review. *Appl. Surf. Sci.* **1982**, *10*, 143–207.

(29) Arblaster, J. W. Crystallographic Properties of Platinum. *Platinum Met. Rev.* **1997**, *41*, 12–21.

(30) Bock, H.; Müller, H. Gas-Phase Reactions. 44. The  $P_4 \rightleftharpoons 2P_2$  Equilibrium Visualized. *Inorg. Chem.* **1984**, *23*, 4365–4368.

(31) Guo, L.; Wu, H.; Jin, Z. First Principles Study of the Evolution of the Properties of Neutral and Charged Phosphorus Clusters. *J. Mol. Struct.: THEOCHEM* **2004**, *677*, 59–66.

(32) Chen, M. D.; Chen, Q. B.; Liu, J.; Zheng, L. S.; Zhang, Q. E.; Au, C. T. Parity Alternation of Ground-State  $P_n^-$  and  $P_n^+$  ( $n = 3 - 15$ ) Phosphorus Clusters. *J. Phys. Chem. A* **2007**, *111*, 216–222.

(33) Powell, C. J.; Jablonski, A. *NIST Electron Effective-Attenuation-Length Database*, 1st ed.; National Institute of Standards and Technology: Gaithersburg, MD, 2001.